Three-dimensional wake transition behind an inclined flat platea)

Dan Yang, Vagesh D. Narasimhamurthy, Bjørnar Pettersen, and Helge I. Andersson

Citation: Physics of Fluids (1994-present) **24**, 094107 (2012); doi: 10.1063/1.4753942
View online: http://dx.doi.org/10.1063/1.4753942
View Table of Contents: http://scitation.aip.org/content/aip/journal/pof2/24/9?ver=pdfcov
Published by the AIP Publishing

Three-dimensional wake transition behind an inclined flat plate[a)]

Dan Yang,[1,b)] Vagesh D. Narasimhamurthy,[2] Bjørnar Pettersen,[1] and Helge I. Andersson[2]
[1]*Department of Marine Technology, Norwegian University of Science and Technology, Trondheim NO-7491, Norway*
[2]*Department of Energy and Process Engineering, Norwegian University of Science and Technology, Trondheim NO-7491, Norway*

(Received 3 March 2012; accepted 25 July 2012; published online 26 September 2012)

Transition phenomena in the wake of a flat plate at 25° angle of attack are investigated by means of three-dimensional computer simulations. The Strouhal number versus Reynolds number relationship was determined for Re from 275 to 800. The Strouhal number turned out to be independent of the Reynolds number for $Re > 400$ and distinctly lower than that reported from recent two-dimensional simulations. A first subharmonic frequency was detected already at $Re = 300$, at which the originally two-dimensional wake also became three-dimensional. The spanwise wavelength of the most energetic three-dimensional mode turned out to be about two times the projected width of the plate and almost independent of Re. The complexities of the vortex shedding increased gradually with increasing Reynolds number until a turbulent-like state with a continuous spectrum of spanwise scales was found. However, while a strict spanwise periodicity was observed for $Re = 350$, a more irregular wake topology occurred at $Re = 325$ with two distinctly different spanwise wavelengths along the span of the plate. The spectral energy of the subharmonic frequency of the longer of these wavelengths was the dominating one. © *2012 American Institute of Physics*. [http://dx.doi.org/10.1063/1.4753942]

I. INTRODUCTION

The bluff body wake flow is a topic of both theoretical and practical importance, due to its relevance in numerous engineering applications. Flow past an inclined flat plate, which represents a high-lift body flow, has proved to be a good choice to represent similar flow features as of both airfoils and hydrofoils.[1,2] The plate inclined at a high angle of attack could provide high lift on the body. The massively separated flow comprises rich dynamic features such as vortex shedding and fluctuating drag and lift forces. These events may lead to flow-induced vibrations, noise generation, and turbulent mixing.

Even behind strictly two-dimensional (2D) bodies, e.g., infinitely long cylinders, the wake flow remains two-dimensional only up to a certain Reynolds number, above which the flow becomes susceptible to three-dimensional (3D) instabilities. This inception of three-dimensionalization of the flow field represents the first stage of a complex transition scenario, which eventually leads to a fully developed turbulent wake. Numerous investigations have been performed in this area experimentally, analytically, and numerically.

Square and circular cylinders are the most commonly used geometries to study the wake transition. The resulting wakes have been investigated and reported in detail by Williamson,[3–6] Barkley and Henderson,[7] Zhang *et al.*,[8] Luo *et al.*,[9,10] and Tong *et al.*[11] Briefly, the square and circular

[a)]This paper is a substantially expanded and refined version of a paper presented by the first author at the 13th European Turbulence Conference (ETC-13) held in Warsaw, Poland, September 2011.
[b)]dan.yang@ntnu.no.

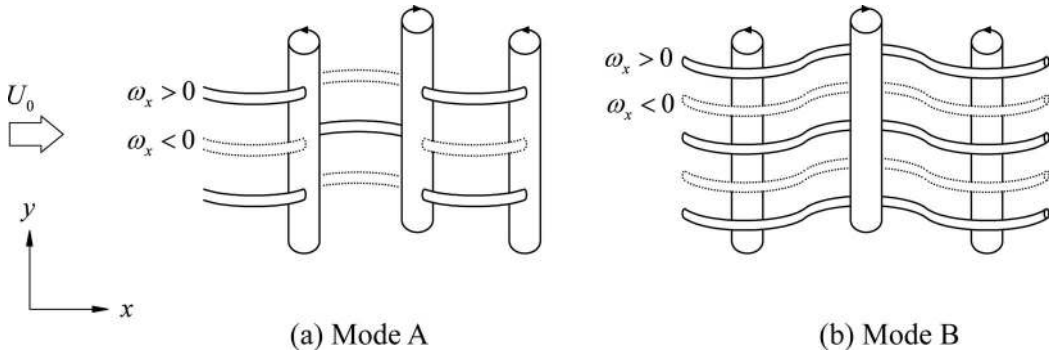

FIG. 1. Schematic representation of mode A and mode B instabilities between rollers. The vortex tubes aligned with the *y*-axis are von Kármán-type roller cells which arise when the near-wake undergoes a Hopf-bifurcation. Adapted from Refs. 14 and 6.

cylinder' wake transition both involves two modes of small-scale three-dimensional instabilities, called mode A and mode B. The critical Reynolds numbers for the inception of these instability modes were identified through the determination of discontinuities in the $St - Re$ curves.

For square cylinder wakes, critical Reynolds numbers of 162 and 190[12] were found for transitions to mode A and mode B instabilities, respectively. These critical Reynolds numbers are lower than their circular cylinder counterparts, which are approximately 188–190 and 230–260[5,7,8,13] for mode A and mode B. The observed spanwise wavelengths for the two modes in square cylinder wakes ($5.22D$ and $1.2D$[12] for mode A and mode B, respectively, where D is the side length of the square cylinder) are longer than their counterparts in circular cylinder flows (3–4 D and 0.8–1 D, respectively, where D is the cylinder diameter). Tong *et al.*[11] investigated the transition phenomena in the wake of an inclined square cylinder, in which mode A and B are present at all six different angles of attack investigated, and the spanwise wavelength shows an angle of attack dependence.

In addition to the spanwise wavelength difference, the streamwise vortex structures in these two dominant modes are quite different, as shown in Fig. 1. In mode A instabilities, vortex loops are formed by drawing away from the rollers at certain spanwise locations.[5] In mode B instabilities, rib-like streamwise counter-rotating vortex loops form the in-line arrangement between the rollers. These structures are distinctly different from mode A instabilities.

Unlike the case of circular or elliptic cylinders, the flow past an inclined flat plate is characterized by fixed separation points at the two edges. The previous works on flow past a flat plate are more focused on the high Reynolds number range and show scarcely relevance to the three-dimensional transition in the wake. For example, one of the earliest experiments performed by Fage and Johanson[15] over a wide range of angles of attack, at Reynolds number of 1.5×10^5, showed that the Strouhal number associated with the vortex shedding scales with the projected width of the plate normal to the incident free-stream. Lam and Leung[16] gave detailed velocity fields obtained with particle-image velocimetry at successive phases of a vortex shedding cycle at angle of attack $20^\circ \sim 30^\circ$, at Reynolds number around 5300.

Flow past a normal flat plate is a common configuration which has been investigated extensively such as Refs. 17–22. According to the short review of Thompson *et al.*[23] the flow past a flat plate with width d normal to the flow undergoes a transition to the two unstable modes at a Reynolds number around 105-110 and 125, with wavelengths of approximately 5–6d and 2d for the two modes.

In the present work, the transition behavior of flow past an inclined flat plate in the Reynolds number range 275–800 is investigated. The angle of attack is chosen as 25° as in Ref. 24. Their two-dimensional simulations show that the transition route from laminar to chaotic flow is particularly complicated at an angle of attack around 20°–30°, which therefore motivate a further focus on the attack angle 25°. Nevertheless, two-dimensional simulations are not the proper candidates to employ while investigating three-dimensional wake transition. The present study is therefore aimed at investigating the data resulting from a fully resolved direct numerical simulation. Some sample results were presented at the 13th European Turbulence Conference.[25] The three-dimensional simulations to be presented in this paper show very complex instabilities at angle of attack 25°.

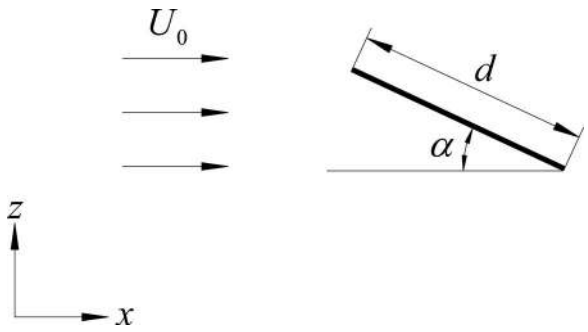

FIG. 2. Sketch of free stream past an inclined flat plate.

This paper is organized as follows: Sec. II presents the flow problem and numerical method used. Section III first illustrates the $St - Re$ relationship from the series of simulations and then the instantaneous vortex structures for different Reynolds numbers. At the end of Sec. III, the spanwise wavelengths are measured from the velocity signals. Finally, Sec. IV presents a brief conclusion.

II. FLOW PROBLEM AND NUMERICAL IMPLEMENTATIONS

We consider the incompressible flow past a flat plate inclined to a uniform free stream, as shown in Fig. 2. The Reynolds number defined in this paper is $Re = U_0 d/\nu$, where U_0 is the free stream velocity, d is the plate width, and ν is the kinematic viscosity. The thickness of the plate is $0.02d$ and the angle of attack is α. We also define the effective Reynolds number $Re' = U_0 d \sin\alpha/\nu$ and the Strouhal numbers $St = fd/U_0$ and $St' = fd \sin\alpha/U_0$ for future use, where f is the dominant wake frequency. The non-dimensional 3D Navier-Stokes equations are expressed as

$$\frac{\partial u_i}{\partial x_i} = 0, \tag{1}$$

$$\frac{\partial u_i}{\partial t} + u_j \frac{\partial u_i}{\partial x_j} = -\frac{\partial p}{\partial x_i} + \frac{1}{Re}\frac{\partial^2 u_i}{\partial x_j \partial x_j}, \tag{2}$$

and are solved directly in time and three-dimensional space. The flow field is described in a Cartesian coordinate system where x is aligned with the free stream direction, y is along the span of the plate, and z is normal to the free stream.

The governing equations are discretized in space by means of the finite-volume method with the grid arranged staggered. The spatial discretization of the convective and diffusive fluxes is based on second-order central differences. The momentum equations are advanced in time by fractional time stepping using a third-order Runge-Kutta scheme in combination with an iterative strongly implicit procedure (SIP) solver for the Poisson equation of pressure. The surface of the arbitrarily inclined plate does not coincide with the Cartesian grid points. To this end, an immersed boundary technique is used. The plate geometry is represented by a triangular mesh. The immersed boundary technique provides a smooth representation of the body surface by using third-order accurate least-squares interpolation for the interface cells.[26] The validation of our code for a normal flat plate has been done in Ref. 20.

The computational domain is $25d \times 6d \times 15d$ in x-, y-, and z-directions, respectively. The upstream and downstream domain sizes are $5d$ and $20d$ with respect to the mid-point of the front face of the plate. The number of grid points is $576 \times 72 \times 450$ with the smallest grid size $0.005d$ around the plate surface. The time step in the simulations is $0.001d/U_0$. The domain size and grid convergence study can be found in Ref. 27.

At the inlet, a uniform free stream velocity profile ($u = U_0$, $v = w = 0$) is assumed. At the outlet boundary, the Neumann boundary condition ($\partial u_i/\partial x = 0$) is used for all the velocity components. No-slip conditions are prescribed all along the plate surface. At the top and bottom boundaries, we adopt the slip-wall condition ($\partial u/\partial z = \partial v/\partial z = \partial p/\partial z = 0$, $w = 0$). In the spanwise direction,

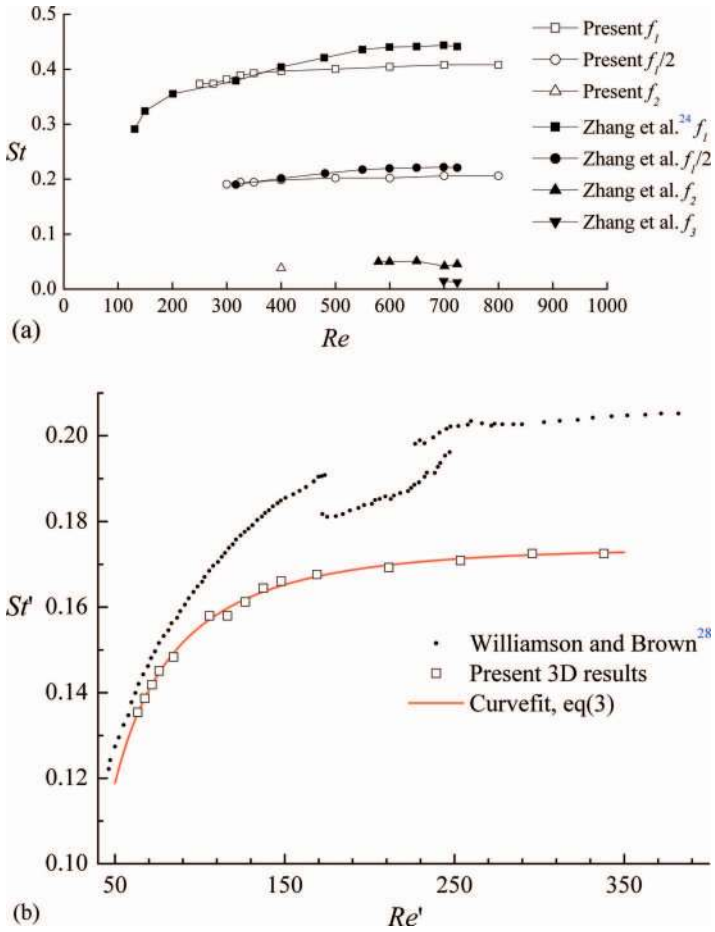

FIG. 3. (a) The $St - Re$ relationship in the wake of an inclined flat plate. The open symbols represent data from the present 3D simulations while the filled symbols are from the 2D simulations by Zhang *et al.*[24] (b) The $St' - Re'$ relationship compared with the $St - Re$ relationship in the wake of a circular cylinder.

periodic boundary conditions are imposed. The simulations are integrated in time for 1000 non-dimensional time units, which correspond to around 380 vortex shedding cycles at $Re = 300$ and 38 low-frequency modulations at $Re = 400$.

III. RESULTS AND DISCUSSION

A series of direct numerical simulations in three dimensions are performed over a range of Reynolds numbers from 275 to 800 for one particular angle of attack, $\alpha = 25°$. Our primary focus of attention is on the lower part of this Re-range, i.e., $Re \leq 400$. The results to be presented aim to elucidate the three-dimensional nature of the transition process. The frequencies that appear in Sec. III are dimensionless values.

A. $St - Re$ relation and velocity-time traces in the wake

The $St - Re$ relation in the Reynolds number range investigated is shown in Fig. 3. For comparison, the 2D numerical data of Zhang *et al.*[24] are also plotted in Fig. 3(a). The discrepancy in the St data arises as the Reynolds number is increased above approximately 400 where the 2D simulations give higher shedding frequencies. The dominant frequencies beyond $Re = 400$ are approximately equal to 0.4, which becomes 0.169 based on the projected width $d' = d \sin\alpha$, over an effective Reynolds number range of $169 \sim 338$. These results are close to the normal flat plate

simulations by Najjar and Balachandar,[17] Saha,[21] and Narasimhamurthy and Andersson,[20] in which the dominant frequencies are $0.161 \sim 0.168$.

Figure 3(b) summarizes the $St' - Re'$ relation which is based on the projected width and compared with the $St - Re$ relationship in the wake of a circular cylinder.[28] The curvefit for the present results could be written as an expansion in $\left(1/\sqrt{Re'}\right)$, i.e.,

$$St' = 0.162 + \frac{0.5111}{\sqrt{Re'}} - \frac{5.773}{Re'}, \tag{3}$$

which is similar to the curvefit for both experimental and numerical $St - Re$ relationships[28] in the wake of a circular cylinder.

In the present simulations, 3D effects appear between $Re = 275$ and $Re = 300$, and at the same time the subharmonic frequency $f_1/2$ is excited. This explains why the present data depart from the 2D simulations by Zhang *et al.*[24] This subharmonic frequency is also excited in the 2D simulations, but then at $Re = 320$.

To gain further insight into the wake transition phenomena, the velocity-time traces and the spectra at some different Reynolds numbers are examined in more detail. The streamwise and crosswise location of the sampling points in Figs. 4–8 are $x/d = 6.0$, $z/d = 8.0$. Figure 4 shows spectra of the velocity components at $Re = 350$. At this Reynolds number the subharmonic $f_1/2$ frequency is excited, as evident in Fig. 4(b). This subharmonic is also observed in the spectrum of the spanwise velocity component in Fig. 4(a), where also peaks corresponding to $3f_1/2$ can be discerned.

Figure 5 shows time traces of the spanwise velocity component at the points located at the frequency wave crests and the wave troughs, in Fig. 4(a). The spanwise velocity oscillates regularly with time at the frequency wave crest (Fig. 5(a)), whereas at the wave trough, the oscillation amplitude of the velocity is substantially smaller and more irregular (Fig. 5(b)).

At $Re = 325$, the spectral energy of the $f_1/2$ subharmonic is not regularly distributed along the span of the plate as it is at $Re = 350$. For the spanwise velocity component, it reduces considerably in the region $4 \lesssim y/d \lesssim 5$ (Fig. 6(a)). The dramatic reduction of the frequency peaks associated with the first subharmonic $f_1/2$ is caused by a yet unexplained suppression of the streamwise-oriented vortices or braids which connect neighboring von Kármán vortex cells, as depicted in Fig. 1. This phenomenon will be further discussed in Subsection III B.

As the Reynolds number is increased in the 2D simulations of Zhang *et al.*,[24] two- and three-frequency (f_2 and f_3) quasi-periodic flow states are generated, for instance, at $Re = 600$ and $Re = 700$. The appearance of these multiple basic frequencies occurs at $Re = 400$ in the present 3D simulations and a wideband spectrum near the $f_1/2$ frequency appears. Figure 7(a) shows the spanwise averaged power spectrum of the crosswise velocity component at $Re = 400$, in which a second basic frequency f_2 is excited. Spectral peaks in Fig. 7(a) occur as linear combinations $m_1(f_1/2) + m_2 f_2$ of the two basic frequencies with m_1 and m_2 as integers.[24] It is noteworthy that frequencies corresponding to $m_2 = 0$ and $m_1 = 1, 2, 3$, and 4 are quite energetic, the latter of which is twice the basic von Kármán frequency f_1. The frequencies found in Fig. 7(a) depend on the different kinds of streamwise and spanwise vortices in the wake. This phenomenon can be connected to the three-dimensional study of Mittal and Balachandar[29] for flow past a circular cylinder. In their study, hairpin structures were formed out of the spanwise rollers. This behavior is associated with the subharmonic frequency in the wake.

Figure 7(b) compares the wideband spectra of spanwise velocity at higher Re with the simple two-frequency spectrum at $Re = 350$. Figure 8 presents the frequency spectrum along the spanwise direction at $Re = 400$. The amplitude variation shows a spanwise modulation with multiple length scales. Comparisons with the corresponding plots in Figs. 4(a) and 6(a) show that the three-dimensionalization of the wake at $Re = 400$ is significantly more irregular than at the somewhat lower Reynolds numbers. However, while the spanwise modulation of the velocity field turned out to be regular at $Re = 350$, an irregular modulation was found at $Re = 325$. While flow complexities normally increase with Re, the flow or wake instabilities need not vary with Re in a linear fashion. Instabilities are known to occur in a specific Reynolds number window and are generally weak

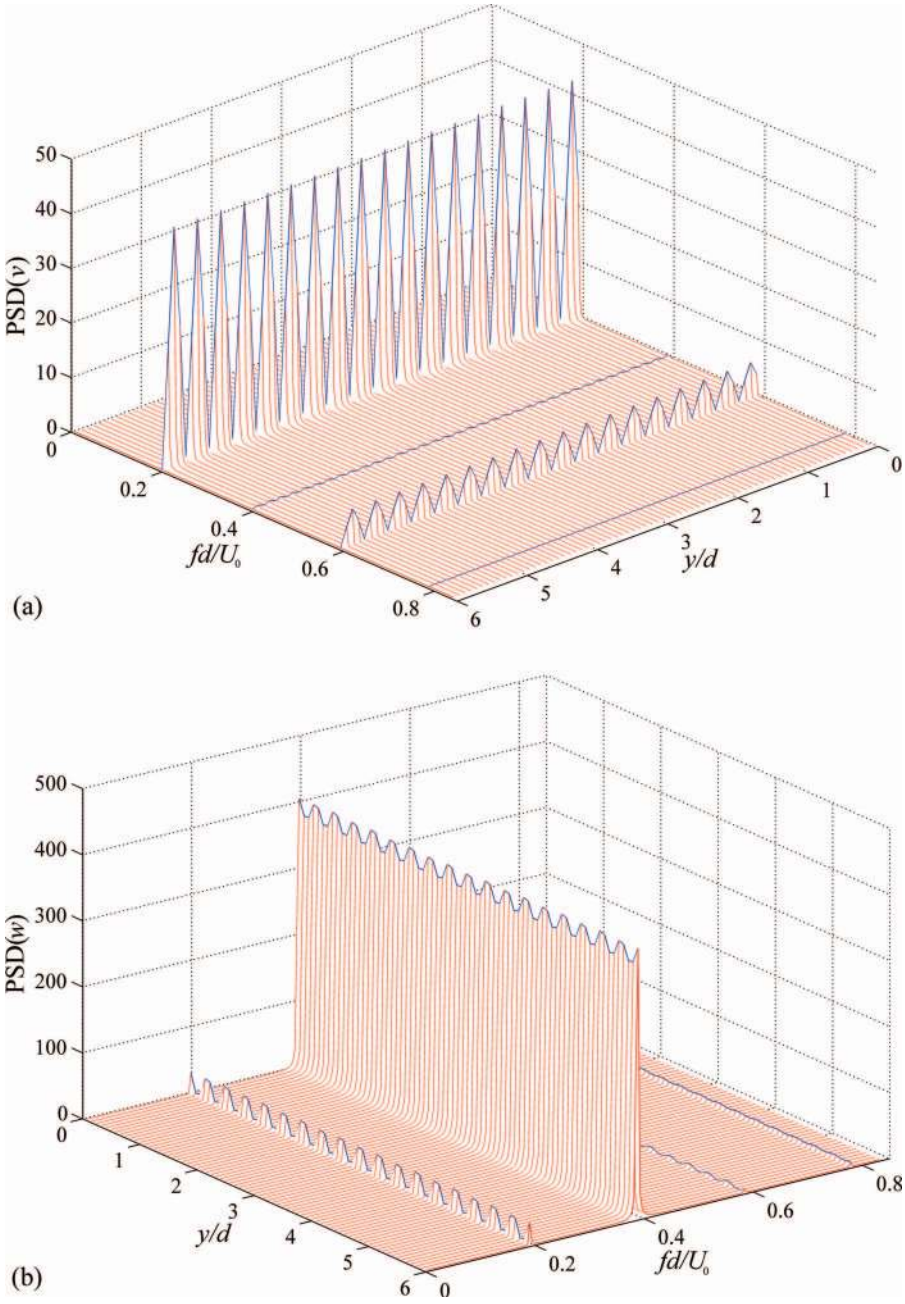

FIG. 4. Spanwise variation of the spectral energy of the wake velocities at $Re = 350$. (a) Spanwise velocity component v; (b) crosswise velocity component w. The lines on the peaks demonstrate the frequency spectral energy oscillation.

during the early stage and gradually stabilize with increasing Re. For example, during the changeover of eddy-shedding mode from mode A to mode B in a circular cylinder wake, i.e., in the Re range of 230–260, the wake is known to be more unstable than at $Re = 300$, where the wake has re-stabilized under the mode B regime.

B. Instantaneous vortex structures

In this section, three-dimensional vortex structures formed in the wake of the inclined flat plate are investigated in detail. At $Re = 350$, the regular streamwise-oriented vortical structures, also

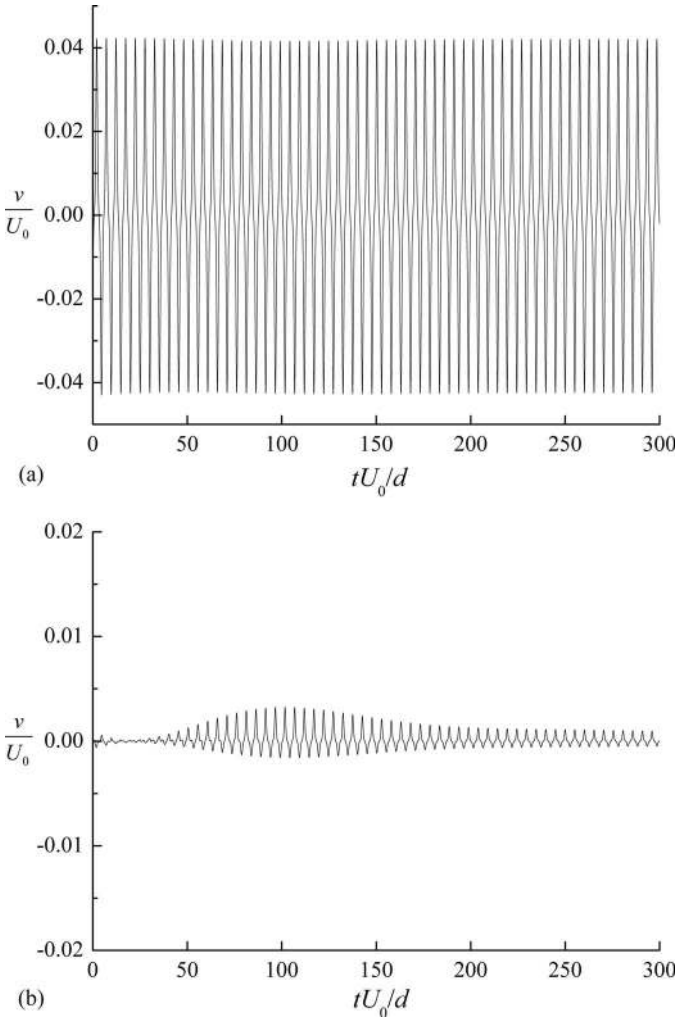

FIG. 5. Spanwise velocity component versus time at $Re = 350$. The tracking position corresponding to the frequency wave crest (a) and wave trough (b). The time-origin $t = 0$ corresponds to a dimensionless time 700.

referred to as braids or ribs, are generated. Figure 9 shows the top view of an instantaneous 3D iso-surface of $-\lambda_2$ at $Re = 350$, which indicates a strict spanwise periodicity. The superiority of the λ_2-method to extract the vortex topology from a three-dimensional flow field is discussed in detail in Ref. 30. The streamwise vortex structures appear repeatedly at the same spanwise location during alternating shedding cycles. This scenario implies a simple spanwise subharmonic behavior, which corresponds to the excitation of the $f_1/2$ frequency.

It should be noted that the spanwise periodicity, at lower Re, is not as regularly distributed in the spanwise direction as it is at $Re = 350$. From the top view at $Re = 325$ in Fig. 10, it is obvious that the periodic structures in the spanwise direction have different length scales. In fact, Fig. 10 indicates two length scales approximately equal to $0.5d$ and $0.8d$, which represent the small and large structures, respectively. The scales of the other structures are distributed between these two values.

Instantaneous plots of the streamwise vorticity ω_x in different cross-sectional (y, z)-planes in the near wake and in the far wake are shown in Figs. 11(a)–11(c) and 11(d)–11(f), respectively. Irregular streamwise vortex distributions occur at every cross section. In the near wake, the streamwise vortex pairs have a shorter length scale in the range $4 \lesssim y/d \lesssim 5$, in which the subharmonic-frequency

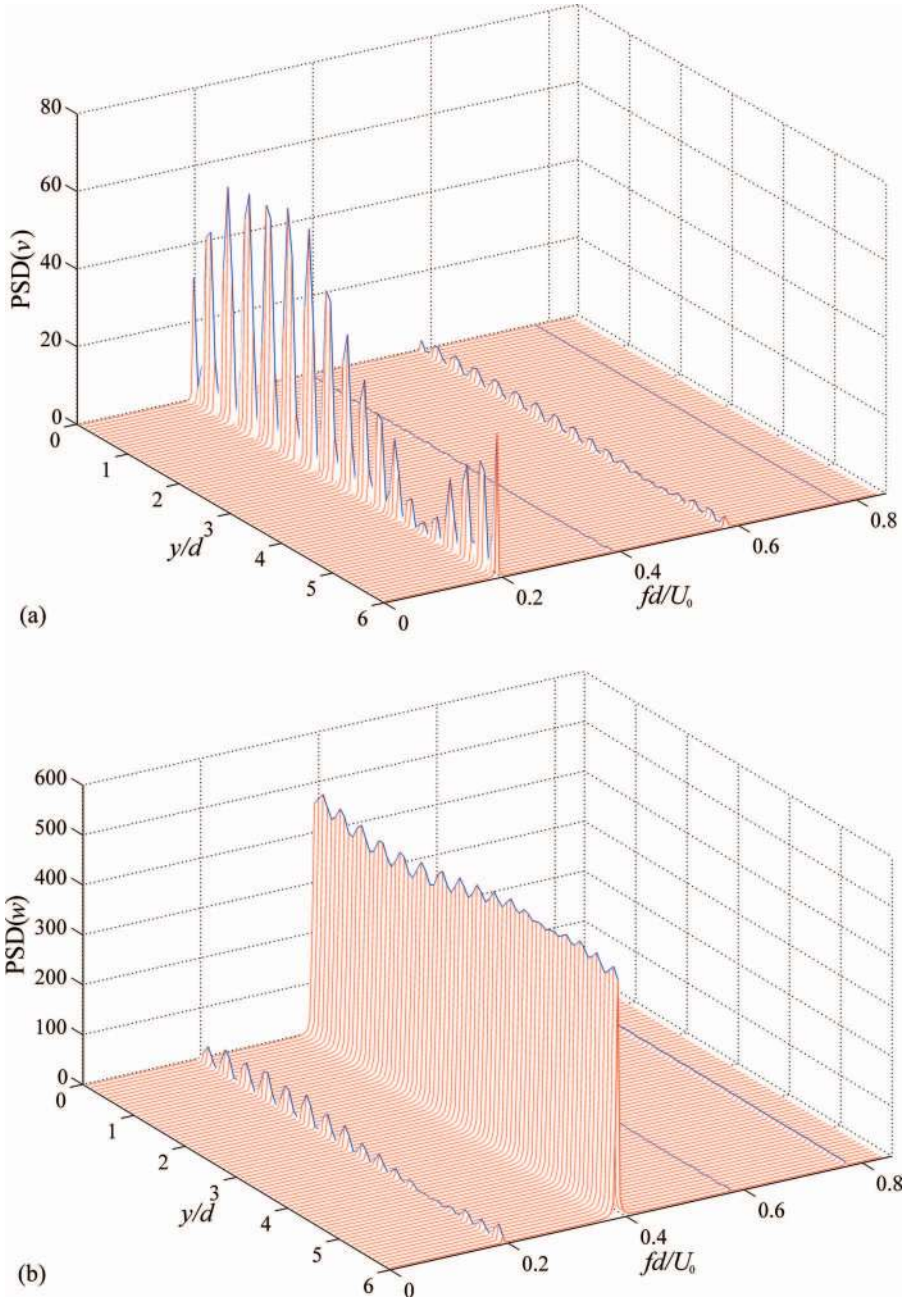

FIG. 6. Spanwise variation of the spectral energy of the wake velocities at $Re = 325$. (a) Spanwise velocity component v; (b) crosswise velocity component w.

spectral energy is very low in Fig. 6(a). On the contrary, the streamwise vortex pairs have a larger length scale in the range $1 \lesssim y/d \lesssim 2$, where the subharmonic-frequency spectral energy is highest.

The side-views of the wake in Fig. 12 show that the streamwise vorticity ω_x at $Re = 325$ is substantially higher in the large-length-scale region in Fig. 12(a) than in the short-length-scale region in Fig. 12(b), i.e., consistent with the cross-sectional plots in Fig. 11. The side-views of the wake at $Re = 350$, on the other hand, reflect the spanwise periodicity of the streamwise vorticity at this particular Reynolds number, as seen also in the top view in Fig. 9. The opposite sign of ω_x in Figs. 12(c) and 12(d) suggests a spanwise periodicity close to two times the distance between the

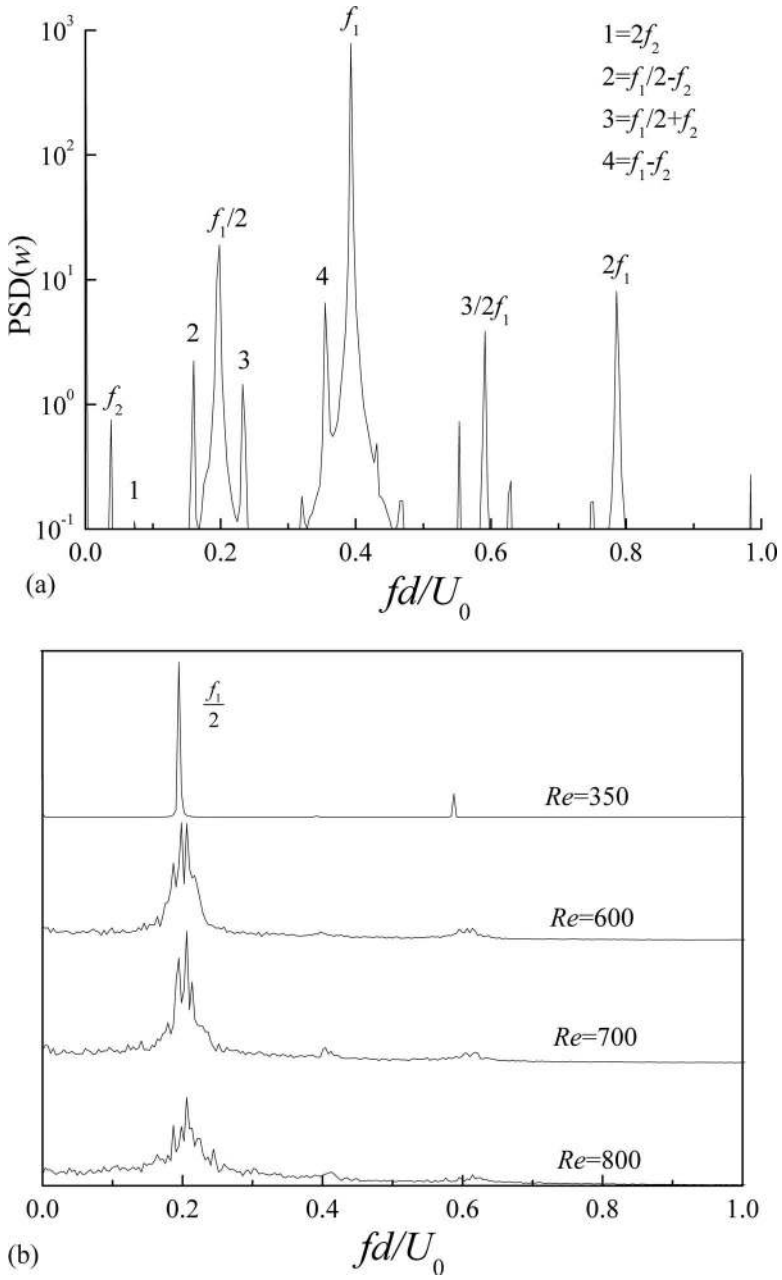

FIG. 7. Spanwise averaged spectra of (a) the crosswise velocity component at $Re = 400$, (b) the spanwise velocity component at different Re.

two (x, z)-planes, i.e., about 0.6d, which is fully consistent with the spanwise periodicity revealed by the λ_2-contours in Fig. 9.

The distribution of the cross-stream vorticity ω_z in the (x, y)-planes near the leading edge and trailing edge are shown in Figs. 13(a) and 13(b), respectively. From the ω_z contours, it is found that ω_z is weak in the small-length-scale region and strong in the large-length-scale region in the wake. These non-equidistant spanwise vortex structures suggest that as Re is lower than 350, the 3D instability mechanism is not sufficiently strong to form identical streamwise structures along the span. At some positions along the plate span, the 3D scales are small and the generated in-line streamwise vortices are very weak. This leads to a discontinuous distribution of the streamwise structures in the wake.

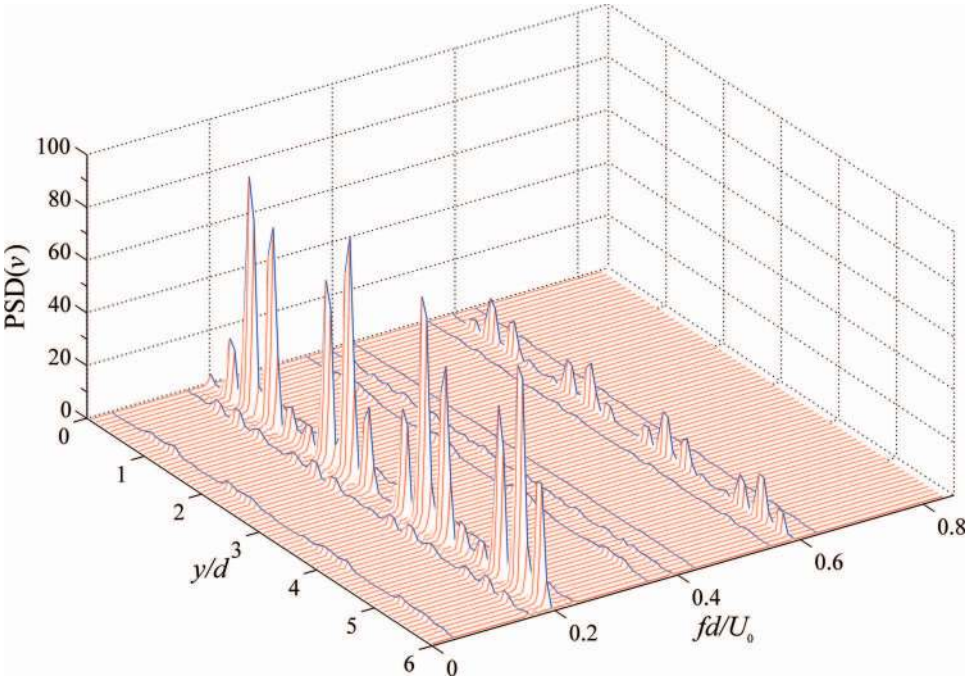

FIG. 8. Spanwise variation of the spectral energy of the spanwise velocity component v, at $Re = 400$.

As the Reynolds number is increased above 400, the complexity of the vortex structures in the wake increases gradually with Re. The plot of the iso-contours of λ_2 in Fig. 14 shows that the vorticity field now possesses multiple length scales co-existing with the quasi-coherent von Kármán cells. The irregularities of the vorticity field in Fig. 14 appear as distinctly different from the quasi-regular topology at $Re = 325$ in Fig. 10 and the strictly regular flow field at $Re = 350$ shown in Fig. 9.

At the highest Reynolds number considered in this study, i.e., $Re = 800$, the wake behind the inclined plate appears as more chaotic than at the lower Reynolds numbers and the spanwise-oriented von Kármán vortices are scarcely visible anymore due to the vigorous three-dimensionalization of the wake. The instantaneous flow field in Fig. 15 closely resembles the wake behind a normal flat plate at $Re = 750$, as studied recently by Narasimhamurthy and Andersson.[20]

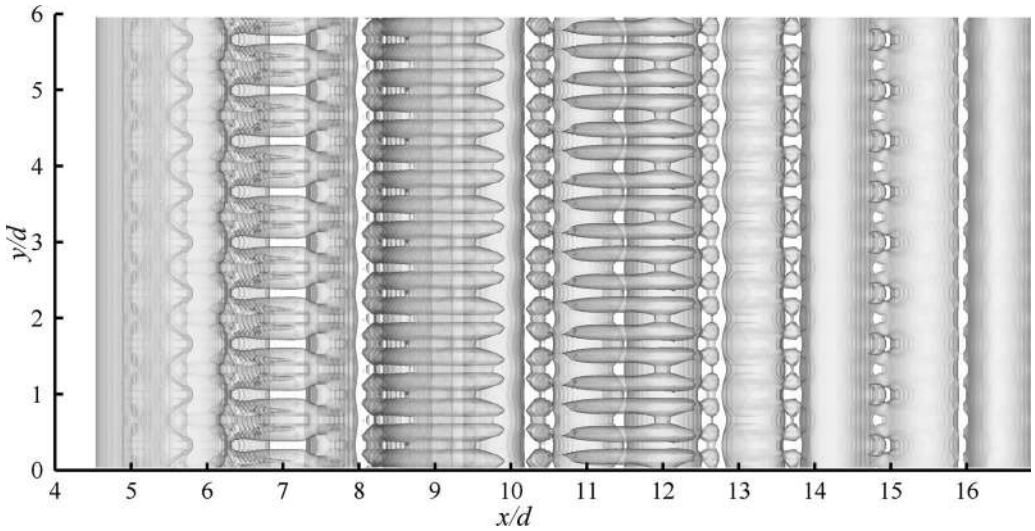

FIG. 9. Instantaneous iso-surface of $-\lambda_2$ at $Re = 350$.

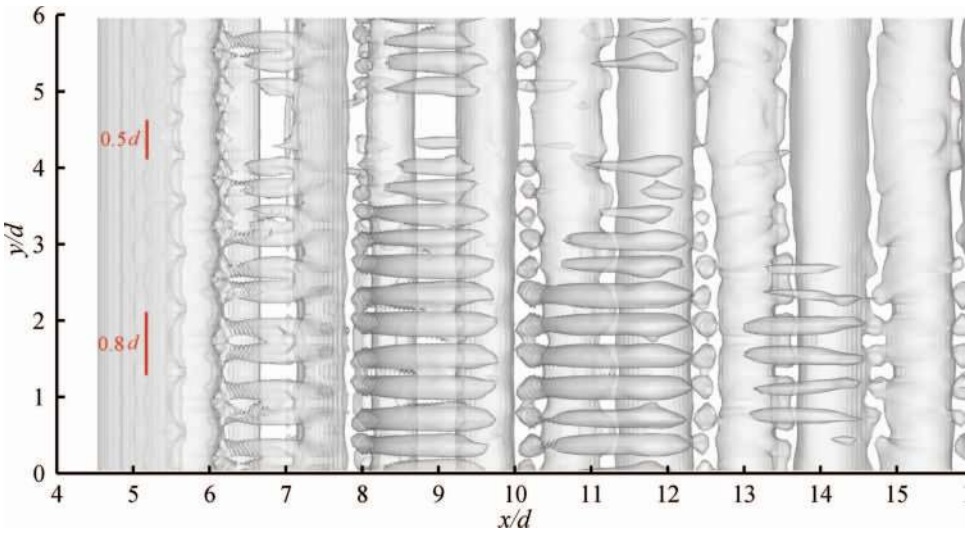

FIG. 10. Instantaneous iso-surface of $-\lambda_2$ at $Re = 325$.

C. Spanwise wavelength

The spanwise wavelength Λ is estimated by means of the two-point correlation function in the spanwise direction. In the present study, the autocorrelation function of the spanwise velocity signal $v(j,t)$ defined as

$$R_{vv}(l,t) = \frac{\frac{1}{N}\sum_{j=1}^{N} v(j,t)\, v(j+l,t)}{\frac{1}{N}\sum_{j=1}^{N} v^2(j,t)} \tag{4}$$

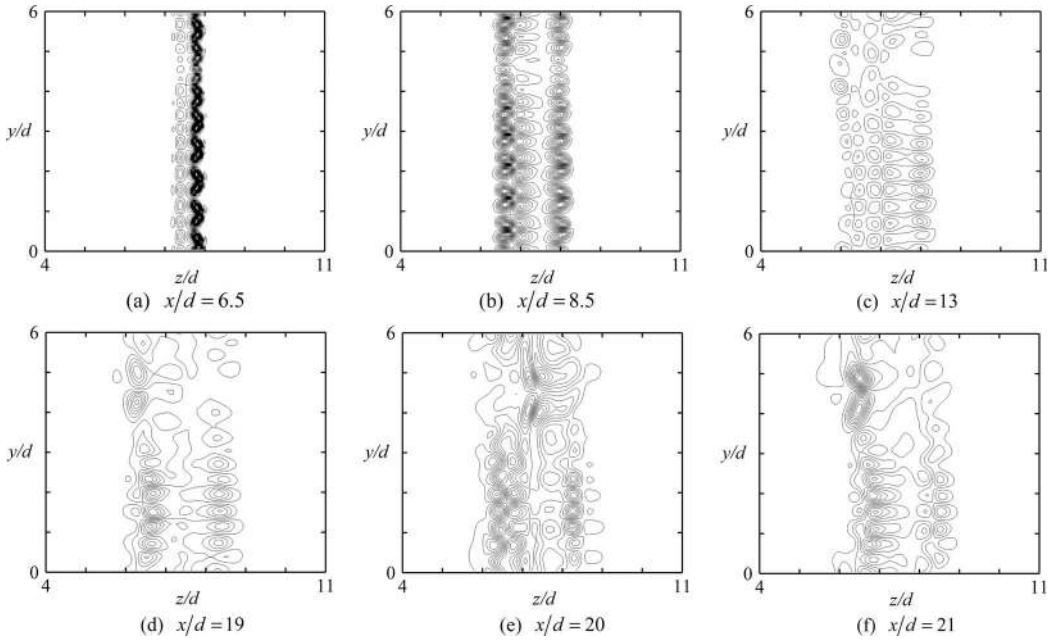

FIG. 11. Contour plots of the streamwise vorticity ω_x in a cross-sectional (y, z)-plane in the near (a)–(c) and far (d)–(f) wake for $Re = 325$. Contour levels are from –4.8 to 4.8 in steps of 0.192 for (a)–(c), and in steps of 0.0384 for (d)–(f).

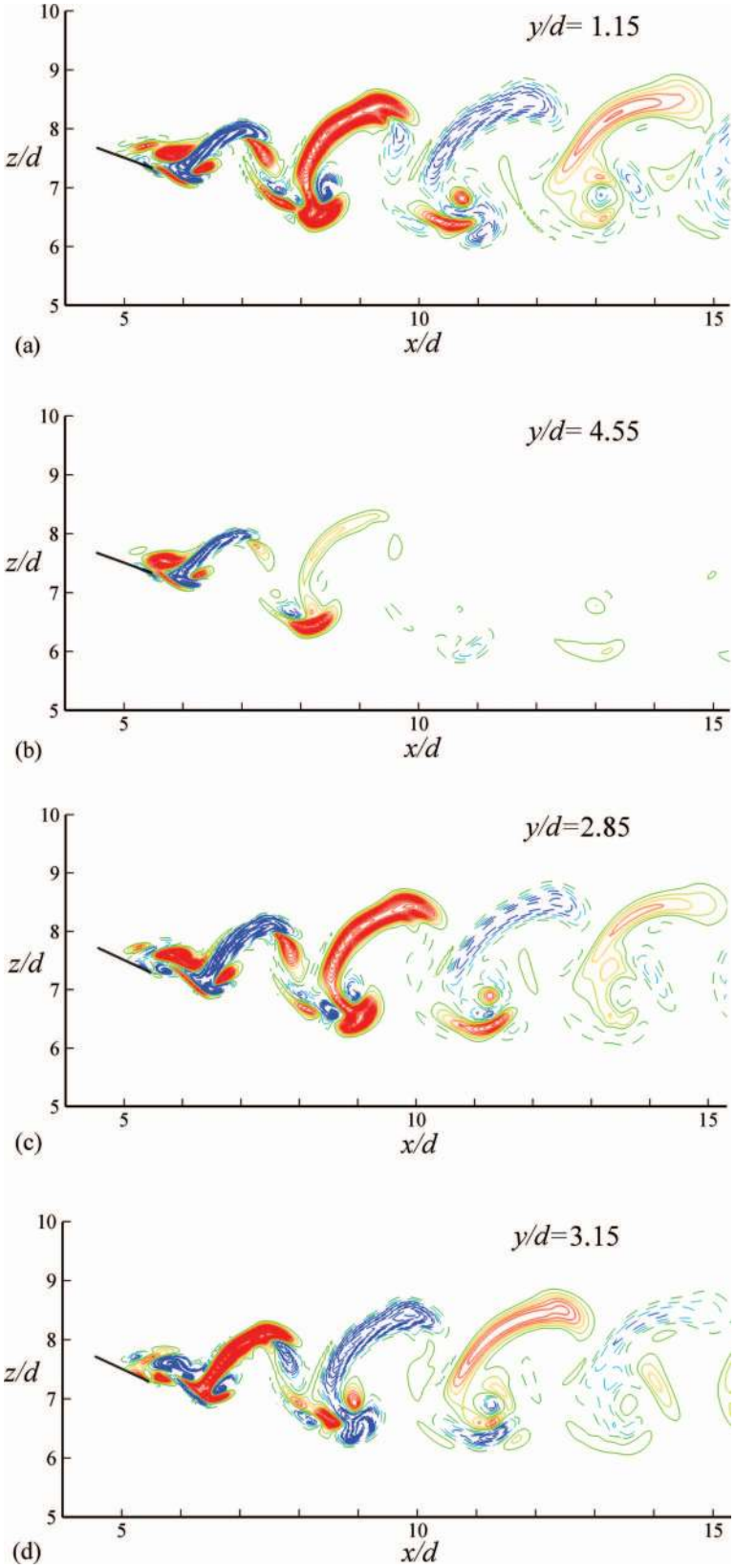

FIG. 12. Side-view of the streamwise vorticity ω_x in the (x, z)-plane at different spanwise positions for $Re = 325$ (a) and (b) and Re = 350 (c) and (d). Contour levels are from –4.8 to 4.8 in steps of 0.1.

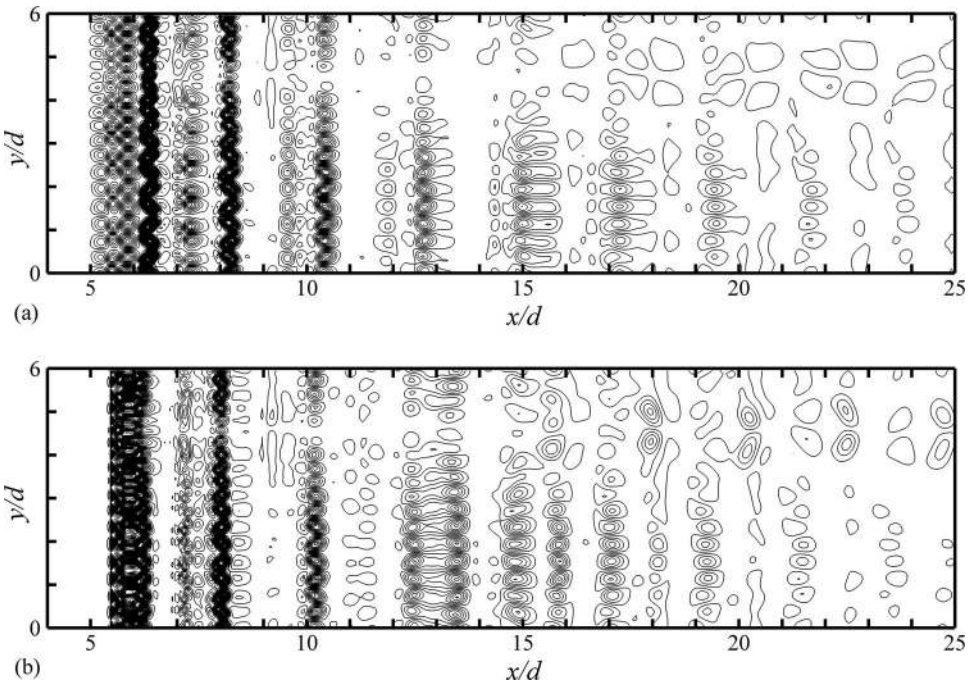

FIG. 13. Contour plots of the cross-stream vorticity ω_z in (x, y)-planes for $Re = 325$. (a) Adjacent to the leading edge of the inclined plate at $z/d = 7.7$; (b) adjacent to the trailing edge at $z/d = 7.3$.

was used to compute the wavelength, $N = 72$ is the number of points per record, and l is the spatial shift. The calculated autocorrelation function was searched for the first maximum, which measured the instantaneous wavelength $\Lambda(t)$. The wavelengths at different Re are obtained by calculating the highest probability of occurrence of $\Lambda(t)$[31] over a time interval of $300d/U_0$. The data shown in Fig. 16 are non-dimensionalized by the projected width $d' = d \sin\alpha$ for the present inclined flat plate case.

Thompson *et al.*[23] indicated that two unstable modes were found in the wake flow past a normal flat plate, i.e., $\alpha = 90^\circ$. These two modes have longer and shorter dominant wavelengths of $\Lambda = 5 - 6d$ and $\Lambda \approx 2d$, respectively. In the present investigation, the spanwise wavelength calculated from the individual time-traces of three different velocity components over the entire Reynolds number range investigated are all distributed around $\Lambda/d' \approx 2.0$ (Fig. 16). This is consistent with the second instability mode A observed by Julien *et al.*[32,33] at $Re \approx 125$, see also the review by Thompson *et al.*[23]

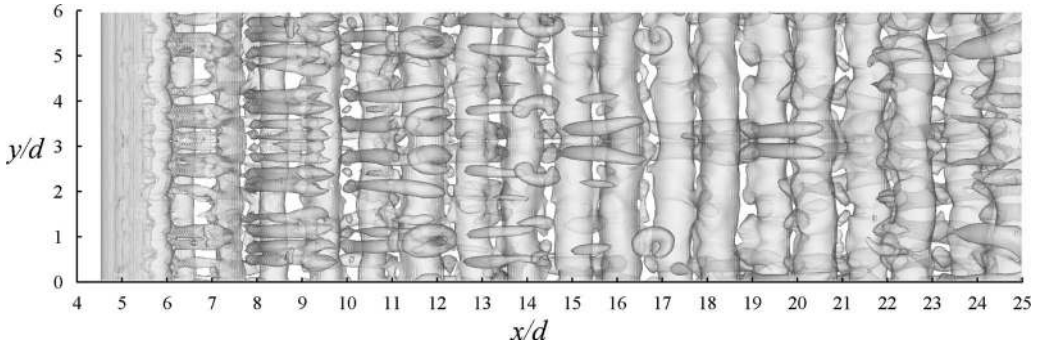

FIG. 14. Instantaneous iso-surface of $-\lambda_2$ at $Re = 400$.

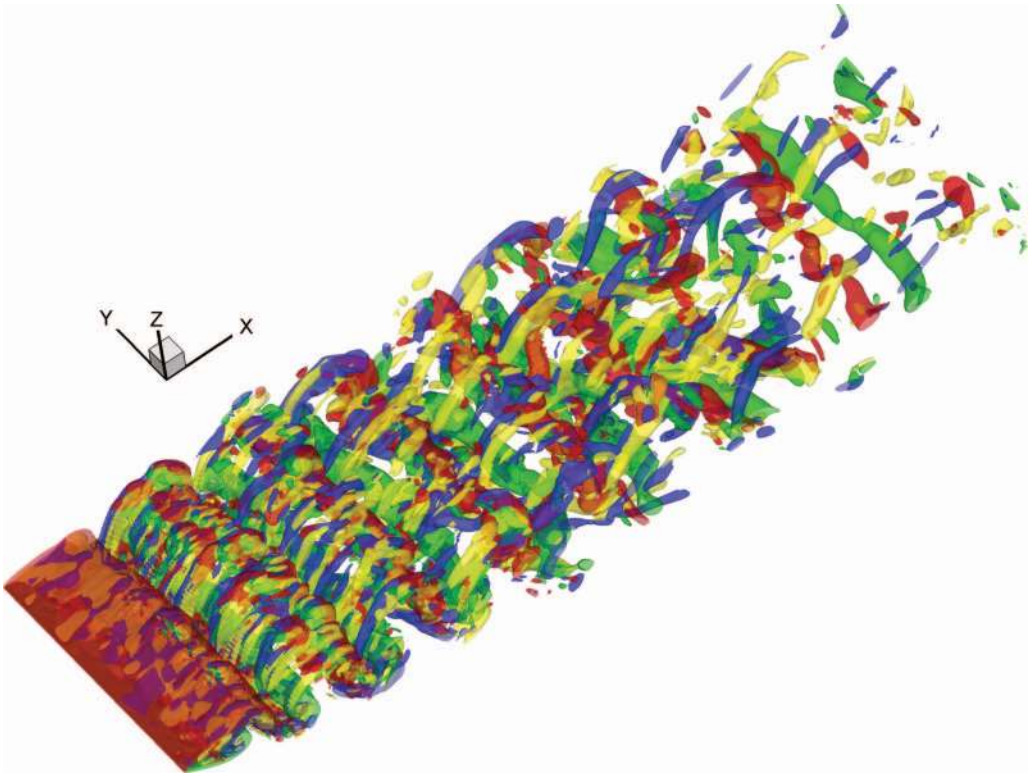

FIG. 15. Perspective view of the streamwise vorticity $\omega_x = \pm 1.0$ (blue and yellow) and spanwise vorticity $\omega_y = \pm 1.0$ (green and red) vortices at $Re = 800$.

Figure 17(a) exhibits the probability density function (PDF) of Λ, which is deduced from the streamwise velocity component at $Re = 400$. From Figs. 3(a) and 7(a) we know that two basic frequencies co-exist at this Re and the other frequency peaks are linear combinations of f_2 and $f_1/2$. The PDF peaks in Fig. 17(a) correspond to $\Lambda = 0.8749$, 1.7701, and 2.7491. The streamwise vortex structures corresponding to these three dominant wavelengths produce the frequency peaks in Fig. 7(a).

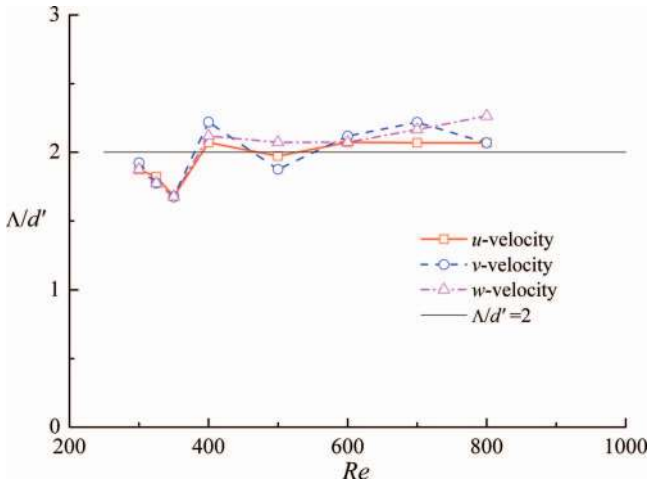

FIG. 16. The spanwise wavelength Λ normalized with the projected plate width $d' = d \sin\alpha$ versus Reynolds number Re at $x/d = 6.0$ and $z/d = 8.0$.

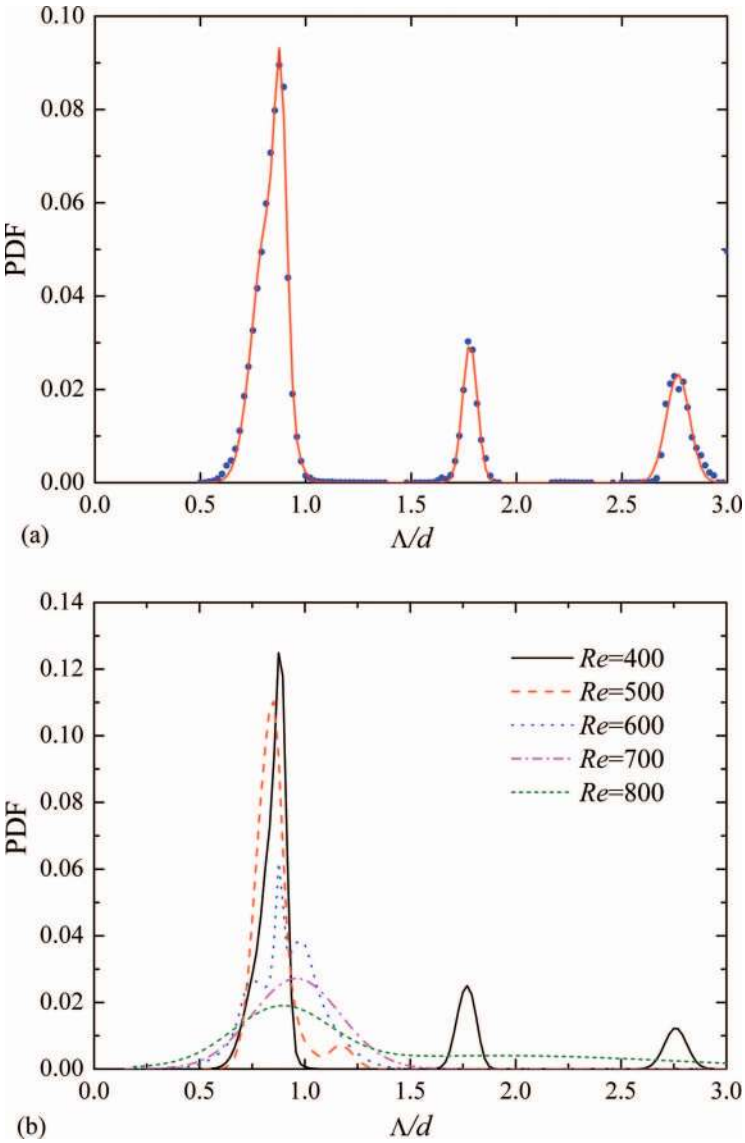

FIG. 17. (a) PDF distribution of spanwise wavelength taken from the streamwise velocity component u at $Re = 400$. The calculated values are shown as discrete points, whereas the lines are curves fitted to the points. (b) Fitting curves of the PDFs at different Reynolds numbers.

The lines in Figs. 17(a) and 17(b) are the fitting curves of the PDFs at different Reynolds numbers. The fitting function is a summation of Gaussian functions with different parameters such as

$$\mathrm{PDF}(\Lambda) = \sum_{i=1}^{n} a_i \exp\left(-\left(\frac{\Lambda - b_i}{c_i}\right)^2\right). \tag{5}$$

The curves in Fig. 17(b) show results fitted to discrete data points for five different Reynolds numbers. The existence of three distinct spanwise wavelengths, as for $Re = 400$, cannot be observed for higher Re. The dominant wavelength $\Lambda \lesssim 1d$, however, seems to persist at all Reynolds numbers, although its signature gradually diminishes with higher Re. At the highest Reynolds number $Re = 800$, a continuous range of spanwise length scales has evolved, in keeping with the notion of a turbulent-like flow field.

IV. CONCLUSIONS

Three-dimensional numerical simulations have been employed to investigate the transition phenomena in the wake of a flat plate, which is inclined to the free stream at an angle of attack of 25°. As the Reynolds number increased above 350, the present numerical results give a nearly constant Strouhal number, which is lower than the two-dimensional simulation results reported earlier by Zhang *et al.*[24] This is rather surprising since the Strouhal number in the wake of a normal flat plate achieves a constant value at a much higher Reynoldes number, i.e., beyond $Re \approx 3000$.[34] At the early stage of the occurrence of the three-dimensional effects, the streamwise vortices are not regularly distributed in the spanwise direction. This is probably due to the relatively low strength of the braid vortices stretching from the spanwise vortex rollers.

As Re is increased to 350, identical pairs of counter-rotating streamwise vortices are formed along the spanwise direction. With further increase of Re, for example, at $Re = 400$, more than one basic frequency is excited and accompanied by multiple dominant spanwise wavelengths. With the variation of Reynolds number, the frequency evolutions of the present 3D simulations reveal a transition process via the sequential occurrence of the period-doubling bifurcations and the various incommensurate bifurcations as indicated by Zhang *et al.*[24]

By using the autocorrelation method, the spanwise wavelength was estimated, from each of the three velocity components and time histories over 300 non-dimensional time units. The calculations indicate that the spanwise wavelength non-dimensionalized by the projected width of the plate, approximately maintains a constant value 2.0 at all Reynolds numbers investigated. This value is in good agreement with the wavelength of the second instability detected in the Floquet analysis of the normal flat plate case.

From the detailed analysis, the transition characteristics in the wake of an inclined flat plate could be described as follows: In the early stage of the transition, the three-dimensional effects are not sufficiently strong to form equivalent streamwise vortices all along the spanwise direction. The Strouhal number initially increases with Reynolds number. As equal-sized secondary vortical structures are formed in the wake, the Strouhal number reaches a constant value. It has been conclusively shown that the spanwise wavelength remains almost constant in the entire three-dimensional transition process, and exhibits a Gaussian distribution about its mean value.

ACKNOWLEDGMENTS

This work has received support from the Research Council of Norway (Program for Supercomputing) through a grant of computing time. We thank the anonymous referees for helpful suggestions.

[1] M. Breuer and N. Jovičić, "Separated flow around a flat plate at high incidence: an LES investigation," J. Turbul. **2**, 1 (2001).
[2] M. Breuer, N. Jovičić, and K. Mazaev, "Comparison of DES, RANS and LES for the separated flow around a flat plate at high incidence," Int. J. Numer. Methods Fluids **41**, 357 (2003).
[3] C. H. K. Williamson, "The existence of two stages in the transition to three dimensionality of a circular cylinder wake," Phys. Fluids **31**, 3165 (1988).
[4] C. H. K. Williamson, "The natural and forced formation of spot-like 'vortex dislocations' in the transition of a wake," J. Fluid Mech. **243**, 393 (1992).
[5] C. H. K. Williamson, "Three-dimensional wake transition," J. Fluid Mech. **328**, 345 (1996).
[6] C. H. K. Williamson, "Vortex dynamics in the cylinder wake," Annu. Rev. Fluid Mech. **28**, 477 (1996).
[7] D. Barkley and R. D. Henderson, "Three-dimensional Floquet stability analysis of the wake of circular cylinder," J. Fluid Mech. **322**, 215 (1996).
[8] H. Zhang, U. Fey, B. R. Noack, M. Konig, and H. Eckelmann, "On the transition of the cylinder wake," Phys. Fluids **7**, 779 (1995).
[9] S. C. Luo, Y. T. Chew, and Y. T. Ng, "Characteristics of square cylinder wake transition flows," Phys. Fluids **15**, 2549 (2003).
[10] S. C. Luo, X. H. Tong, and B. C. Khoo, "Transition phenomena in the wake of a square cylinder," J. Fluids Struct. **23**, 227 (2007).
[11] X. H. Tong, S. C. Luo, and B. C. Khoo, "Transition phenomena in the wake of an inclined square cylinder," J. Fluids Struct. **24**, 994 (2008).
[12] J. Robichaux, S. Balachandar, and S. P. Vanka, "Three-dimensional Floquet instability of the wake of square cylinder," Phys. Fluids **11**, 560 (1999).

[13] O. Posdziech and R. Grundmann, "Numerical simulation of the flow around an infinitely long circular cylinder in the transition regime," Theor. Comput. Fluid Dyn. **15**, 121 (2001).
[14] M. Brede, H. Eckelmann, and D. Rockwell, "On secondary vortices in the cylinder wake," Phys. Fluids **8**, 2117 (1996).
[15] A. Fage and F. C. Johansen, "On the flow of air behind an inclined flat plate of infinite span," Proc. R. Soc. London, Ser. A **116**, 170 (1927).
[16] K. M. Lam and M. Y. H. Leung, "Asymmetric vortex shedding flow past an inclined flat plate at high incidence," Eur. J. Mech. B/Fluids **24**, 33 (2005).
[17] F. M. Najjar and S. Balachandar, "Low-frequency unsteadiness in the wake of a normal flat plate," J. Fluid Mech. **370**, 101 (1998).
[18] F. M. Najjar and S. P. Vanka, "Effects of intrinsic three-dimensionality on the drag characteristics of a normal flat plate," Phys. Fluids **7**, 2516 (1995).
[19] F. M. Najjar and S. P. Vanka, "Simulations of the unsteady separated flow past a normal flat plate," Int. J. Numer. Methods Fluids **21**, 525 (1995).
[20] V. D. Narasimhamurthy and H. I. Andersson, "Numerical simulation of the turbulent wake behind a normal flat plate," Int. J. Heat Fluid Flow **30**, 1037 (2009).
[21] A. K. Saha, "Far-wake characteristics of two-dimensional flow past a normal flat plate," Phys. Fluids **19**, 128110 (2007).
[22] S. J. Wu, J. J. Miau, C. C. Hu, and J. H. Chou, "On low-frequency modulations and three-dimensionality in vortex shedding behind a normal plate," J. Fluid Mech. **526**, 117 (2005).
[23] M. C. Thompson, K. Hourigan, K. Ryan, and G. J. Sheard, "Wake transition of two-dimensional cylinders and axisymmetric bluff bodies," J. Fluids Struct. **22**, 793 (2006).
[24] J. Zhang, N.-S. Liu, and X.-Y. Lu, "Route to a chaotic state in fluid flow past an inclined flat plate," Phys. Rev. E **79**, 045306 (2009).
[25] D. Yang, B. Pettersen, H. I. Andersson, and V. D. Narasimhamurthy, "Three-dimensional transition to turbulence in the wake of an inclined flat plate," J. Phys.: Conf. Ser. **318**, 032044 (2011).
[26] N. Peller, A. L. Duc, F. Tremblay, and M. Manhart, "High-order stable interpolations for immersed boundary methods," Int. J. Numer. Methods Fluids **52**, 1175 (2006).
[27] D. Yang, B. Pettersen, H. I. Andersson, and V. D. Narasimhamurthy, "Vortex shedding in flow past an inclined flat plate at high incidence," Phys. Fluids **24**, 084103 (2012).
[28] C. H. K. Williamson and G. L. Brown, "A series in $1 / \sqrt{Re}$ to represent the Strouhal-Reynolds number relationship of the cylinder wake," J. Fluids Struct. **12**, 1073 (1998).
[29] R. Mittal and S. Balachandar, "Generation of streamwise vortical structures in bluff body wakes," Phys. Rev. Lett. **75**, 1300 (1995).
[30] J. Jeong and F. Hussain, "On the identification of a vortex," J. Fluid Mech. **285**, 69 (1995).
[31] H. Mansy, P.-M. Yang, and D. R. Williams, "Quantitative measurements of three-dimensional structures in the wake of a circular cylinder," J. Fluid Mech. **270**, 277 (1994).
[32] S. Julien, J. Lasheras, and J.-M. Chomaz, "Three-dimensional instability and vorticity patterns in the wake of a flat plate," J. Fluid Mech. **479**, 155 (2003).
[33] S. Julien, S. Ortiz, and J.-M. Chomaz, "Secondary instability mechanisms in the wake of a flat plate," Eur. J. Mech. B/Fluids **23**, 157 (2004).
[34] I. P. Castro and P. Rogers, "Vortex shedding from tapered plates," Exp. Fluids **33**, 66 (2002).